Received: 9 August 2021 | Revised: 4 August 2022 | Accepted: 3 September 2022

DOI: 10.1111/jmg.12702

ORIGINAL ARTICLE

Journal of METAMORPHIC GEOLOGY WILEY

Partial melting and reaction along deformation features in plagioclase

Sarah Incel[1,2] | **Marie Baïsset**[3] | **Loïc Labrousse**[3] | **Alexandre Schubnel**[4]

[1]Institute for Geology, Mineralogy, and Geophysics, Ruhr-Universität Bochum, Bochum, Germany

[2]Department of Materials, Imperial College London, South Kensington Campus, London, UK

[3]Sorbonne Université, CNRS-INSU, Institut des Sciences de la Terre Paris, ISTeP, UMR7193, Paris, France

[4]Laboratoire de Géologie de l'ENS - PSL Research University - UMR8538 du CNRS, Paris, France

Correspondence
Sarah Incel, Department of Materials, Imperial College London, South Kensington Campus, London SW7 2AZ, UK.
Email: sincel@imperial.ac.uk

Handling Editor: Dr. Katy Evans

Funding information
European Research Council, Grant/Award Number: 2016-grant 681346; Alexander von Humboldt-foundation

Abstract

Geological processes involving deformation and/or reactions are highly influenced by the rock grain size, especially if diffusion-controlled processes take place such as metamorphic reactions and diffusion creep. Although many processes, inducing grain-size reduction, are documented and understood at relatively high stresses and low temperatures (e.g., cataclasis) as well as at lower stress and higher temperature conditions (e.g., bulging and subgrain rotation), deformation twinning, a plastic deformation mechanism active in various minerals at lower temperatures, has been neglected as nucleation site for melting and reaction and thus as a cause for grain-size reduction so far. We conducted experiments on natural plagioclase-bearing aggregates at 2.5 to 3 GPa confining pressure and temperatures of 700°C to 950°C using two different deformation apparatus, a deformation multianvil apparatus (DDIA) and a Griggs press, as well as a piston-cylinder apparatus. Regardless of the apparatus type, we observe the breakdown of plagioclase into an eclogite-facies paragenesis, which is associated with partial melting in the high temperature domain of the eclogite facies. Partial melting mostly takes place along the grain and interphase boundaries. However, several melt patches or plagioclase decomposition products coincide with the occurrence of deformation twins and grain-scale microcracking in plagioclase indicating intracrystalline melting and reaction in addition to melting and reaction along grain and interphase boundaries. In the present study, we demonstrate how the interplay between brittle microcracking and plastic deformation twinning can cause intracrystalline melting and/or reaction, which has the potential to lower the effective grain size of plagioclase-rich rocks and thus impacts their reactivity and deformation behaviour.

KEYWORDS
continental crust, deformation twinning, partial melting, plagioclase deformation, semibrittle regime

1 | INTRODUCTION

Partial melting under eclogite-facies conditions, and especially under Ultra High Pressure (UHP) conditions, has been documented from the Central Alps (Pellegrino et al., 2020), the Bohemian Massif (Ferrero et al., 2015), the Western Gneiss Region in Norway to the North Qaidam (Cao et al., 2019), and the central Sulu mountain belt in China (Wang et al., 2020). It has been shown experimentally that the strength of plagioclase-rich rocks dramatically drops at melt fractions ϕ between 0.0 and 0.07 (Rosenberg & Handy, 2005). Partial melting in the UHP domain is therefore expected to dramatically change force balance within collision wedges.

Plagioclase minerals (comprising ∼39 vol.%) are the most common rock-forming mineral group of Earth's crust (Klein, 2001). Rocks such as gabbros, basalts, anorthosites, and granulites can consist almost entirely of plagioclase feldspars, and in granites, granodiorites, and tonalites, common rock types of the continental crust, plagioclase feldspar is a major phase besides quartz and alkali-feldspar. Therefore, the deformation behaviour of these rocks, but also the chemical reactions taking place in them, will depend on the physical and chemical properties of plagioclase. Besides studies investigating the mechanical behaviour of plagioclase-rich rocks over a broad pressure (P) temperature (T)–strain rate ($\dot{\varepsilon}$) range (Fukuda et al., 2018; Fukuda et al., 2022; Rybacki et al., 2006; Rybacki & Dresen, 2004; Tullis, 2018; Tullis & Yund, 1992, 1987), there are also studies focusing on the impact of plagioclase breakdown at high pressure (HP) conditions. This decomposition of plagioclase at HP is considered as one of the most important metamorphic reactions in the crust, and the modalities of its breakdown directly control the mechanical behaviour of the reacting rock (Stünitz & Tullis, 2001). The metastability of plagioclase under eclogite-facies conditions has been widely documented in subducted continental units (Austrheim, 1986; John & Schenk, 2003; Schorn & Diener, 2017), and the first steps of eclogitization at HP conditions actually relate to the triggering of its destabilization in the presence of water. Understanding how plagioclase reacts at HP conditions is therefore a first-order step towards understanding of mechanical behaviour changes in the subducting crust.

Besides P, T, $\dot{\varepsilon}$, and water fugacity, grain size also has a tremendous influence on a rock's mechanical behaviour as well as on the onset and progress of metamorphic reactions. In most systems, deformation and reaction are closely coupled. Metamorphic reactions can transiently decrease the grain size of a rock (Jamtveit et al., 2009; Putnis et al., 2007; Røyne et al., 2008) and therefore influence its deformation behaviour (Renner et al., 2002). Moreover, some deformation processes result in grain-size reduction and thus increase the reactive surface area. Among these mechanisms, cataclasis is acknowledged in the low temperature–high stress regime and can lead to cataclastic flow (Passchier & Trouw, 2005). At higher temperatures and lower stress, crystal plastic deformation can lead to grain-size reduction by dynamic recrystallization. Dislocation glide can result in subgrain rotation which is considered as a first-order mechanism for creep in low temperature mylonites (Hirth & Tullis, 1992; Stipp et al., 2002). Deformation twin or twin boundaries in general have been discussed as possible planes of weakness facilitating crack propagation leading to grain-scale fracturing in the brittle or semibrittle field (e.g., Tullis & Yund, 1992, p. 107). Yet, in situations in which crystal plastic deformation dominates, recovery of deformation twins by twin boundary migration recrystallization will not result in grain-size reduction (Passchier & Trouw, 2005).

Plagioclase is known for its extensive polysynthetic twinning. Polysynthetic twins are caused by interruptions during grain growth (e.g., Cahn, 1954, ch. 2.1.3.3; Smith & Brown, 1988, ch. 18). Further, plagioclase is able to form twins under stress resulting in the formation of so-called mechanical or deformation twins (Borg & Heard, 1969; Marshall & McLaren, 1977; Smith & Brown, 1988, ch. 18). There are two deformation twin systems in plagioclase-producing albite twins, with (010) as the twin plane, and pericline deformation twins, with [010] as the twin axis and the so-called "rhombic section" as the twin plane (Smith & Brown, 1988, ch. 18). Deformation twins form when a critical shear stress is resolved along the relevant crystallographic planes and directions in plagioclase. Microscopically, growth and deformation twins can be differentiated based on their shape. Growth twins mostly strike through the entire grain and form parallel twin boundaries, whereas deformation twins show a lenticular form and affect only a small volume of the grain. In most cases, deformation twins are limited by grain boundaries, cracks, or other lattice defects that act as stress heterogeneities (Cahn, 1954, ch. 3.1.9 and 3.2.5). Thus, besides grain or interphase boundaries, plagioclase exhibits numerous other interfaces such as growth and deformation twin boundaries.

In the present experimental study, we show that the breakdown of plagioclase at eclogite-facies conditions can start with partial melting not only along grain and/or interface boundaries but also along cleavage cracks and deformation twin boundaries. The exploitation of deformation features for melting and reaction ultimately leads to a much lower effective grain size compared with the same processes when solely restrained to grain boundaries.

2 | MATERIALS AND METHODS

2.1 | Sample preparation, characterization of the starting material, and thermodynamic modelling

Experiments were conducted on a granulite-drill core or on granulite powders obtained by crushing and grinding of a mafic granulite from Holsnøy, SW Norway (60°31′57.7″ N, 5°07′14.5″ E). Additional information on the drill core is given by Incel et al. (2020). After grinding, the powder was sieved using a mesh width of 38 μm and washed using distilled water to remove dust. Once dried, the final granulite powder served as starting material for the experiments and consists almost exclusively of plagioclase (~90 vol.%) showing intermediate composition ($anorthite_{47}albite_{52}orthoclase_1$). The remaining 10 vol.% consists of clinopyroxene and orthopyroxene (Opx; Cpx), spinel (Spl), corundum (Crn), and epidote group minerals (Ep) intergrown with alkali-feldspar (Afs; mineral abbreviations follow Whitney & Evans, 2010). Occasionally, garnet (Grt), quartz (Qz), phlogopite (Phl), and amphibole (Amp) grains can be found. Thermodynamic modelling was conducted using Perple_X (Connolly, 1990). The thermodynamic database used was from Holland and Powell (1998), and we chose melt (HP), Gt (HP), Pl(h), Pheng (HP), and Omph (HP) as solution models (Holland & Powell, 1996, 1998, 2001, 2003; White et al., 2001).

2.2 | Experimental and analytical methods

For the current study, we used three different deformation apparatus, a deformation multianvil apparatus (DDIA) press and two different Griggs apparatus, as well as a piston-cylinder press. The DDIA apparatus used for this study is mounted on the 13 BM-D beamline at the Advanced Photon Source, National Laboratory Argonne, Il, USA. Prior to deformation, the samples were hot pressed at 2.5 GPa and ~720°C for 1 h. Then, deformation was initiated by advancing the upper and bottom pistons at a constant rate in displacement-controlled mode. During deformation, the DDIA sample (NG_2.5_1225 in Incel, Labrousse, et al., 2019) experienced syndeformational heating in three steps from ~720°C to 850°C at 14% strain, to ~900°C at 23% strain, and to the final temperature of ~950°C at 30% strain after which the sample was quenched by cutting off the power supply for the graphite furnace. The total axial strain was 34% and deformation lasted ~2 h. The effective strain rate on the sample was $\sim 5{\cdot}10^{-5}$ s^{-1}. Temperatures were calculated by offline calibrations, and uncertainties are below 10% (Hilairet et al., 2012). Details on the sample assembly used, as well as on the calculation of the strain, strain rate, and differential stress, are given by Incel et al. (2017) and Incel, Labrousse, et al. (2019). Further details on the experimental setup can be found in Wang et al. (2003). We performed another deformation test using the same powder in a Griggs deformation rig at constant pressure and temperature conditions of 2.5 GPa and ~700°C and a deformation rate of $4{\cdot}10^{-6}$ s^{-1}. Information about the sample assembly used can be found in Moarefvand et al. (2021). A second experiment was conducted in another Griggs apparatus at 2.5 GPa at 900°C. The strain rate was $\sim 5{\cdot}10^{-5}$ s^{-1}. In contrast to the other deformation tests, these Griggs tests were conducted using the granulite-drill core ("as-is" sample deformed at 2.5 GPa and 900°C to ~35% strain in Incel et al., 2020). Further details on the apparatus and the sample assembly used can be found in Rybacki et al. (1998). In order to test the influence of deformation on plagioclase microstructures, we conducted an additional experiment under static pressure conditions using a piston-cylinder press. The sample remained under 3 GPa and 950°C for ~24 h. The experimental conditions for every run and the sample nomenclature are listed in Table 1. The Griggs experiments were performed in the Experimental Geophysics Laboratory at Ruhr-Universität Bochum, Germany, and in the Laboratoire de Géologie at Ecole Normale Supérieure Paris, France. The piston-cylinder experiments were performed at the Institut de Physique du Globe Paris, France.

The recovered samples were embedded in epoxy, cut lengthwise, polished, and carbon coated for microstructural analyses in the scanning-electron microscope

TABLE 1 Experimental conditions

Sample	Press	Starting material	*P* (GPa)	*T* (°C)	Strain rate (s^{-1})	Total strain (%)
D_2.5_720-950	DDIA	Powder	2.5	720–950	$5{\cdot}10^{-5}$	35
G_2.5_700	Griggs	Powder	2.5	700	$4{\cdot}10^{-6}$	28
G_2.5_900	Griggs	Drill core	2.5	900	$5{\cdot}10^{-5}$	35
P_3_950	Piston cylinder	Powder	3.0	950	—	—

Abbreviation: DDIA, deformation multianvil apparatus.

(SEM). The SEM analyses include low- and high-magnification images taken in backscatter electron (BSE) mode, energy-dispersive X-ray spectroscopy (EDX), and electron-backscatter diffraction (EBSD). The BSE images were taken at an acceleration voltage of 20 kV, and the EBSD maps were acquired with an acceleration voltage of 10 kV and a step or pixel size of 0.5 μm. The EBSD data were processed using the open-source crystallographic toolbox MTEX (Bachmann et al., 2010). We considered non-indexed pixels to have a mean angular deviation value <1 and non-indexed grains to contain less than 2 indexed pixels (<1 μm). Twin boundaries were detected with misorientation angles >178°.

3 | RESULTS

In the SEM, the recovered samples from deformation tests on a powdered starting material show numerous areas that are appearing darker than the surrounding plagioclase matrix in BSE mode (Figures 1–5). These dark zones exhibit small vesicles (Figures 1f, 2a, and 3a) and coincide with non-indexed areas indicating that they are either poorly crystalline or consist of grains with a grain size smaller than the step size used for the analyses (Figures 3b–d and 5b). Further, interaction with the electron beam causes the formation of alteration haloes in these zones (Figures 3a and 5a). BSE images and EBSD analyses demonstrate that although most of these areas are restricted to grain or interphase boundaries and show no particular shape, some also appear to have penetrated plagioclase grains along specific directions or formed patch-like features, commonly with sharp edges oriented ±45° relative to the direction of maximum compression (σ_1; Figures 1b, 2a, 3, and 5). The host plagioclase around these patches shows no to very little difference in orientation as highlighted by an Euler map and inverse pole figures (Figure 3). Schmid factor maps demonstrate that the dark, non-indexed zones often coincide with the presence of albite-deformation twins in plagioclase (Figure 5b,c), which formed in favourably oriented plagioclase grains with respect to σ_1 during deformation (Figures 4b, black arrows, and 5d). However, also grains that are less favourably oriented for deformation twinning (greenish colours) reveal the presence of deformation twins spatially associated with non-indexed areas (red arrows in Figure 4b). Grains that are ideally oriented for deformation twinning appear to be slightly larger than the unfavourably oriented plagioclase grains (blueish colours in Figure 4b). Regardless of the location of these dark-appearing zones, that is, within plagioclase grains or surrounding them, they are commonly spatially associated with areas showing a higher microcrack density relative to the surrounding plagioclase-host grain or plagioclase matrix (Figures 1c,d and 4b,c). In sample D_2.5_720-950, at low magnification, most zones, showing a high microcrack density and the appearance of dark zones, form a band oriented at ~45° towards σ_1 (Figure 1a).

Phase maps and EDX analyses together with element distribution maps demonstrate the growth of mostly omphacite (Omp) and Ep, which sometimes forms euhedral-shaped grains, within the dark, non-indexed zones along the grain and interphase boundaries as well as along deformation twins (Figures 5a). Some patches reveal the growth of sub-euhedral Qz grains within the patches (Figures 1b and 2a). A composite image of K, Na, and Ca element distribution maps and a Si-distribution map demonstrate that the material surrounding the Qz grains, which fills the patch, is richer in K and Si than the initial plagioclase composition (Figure 2b,c). The plagioclase matrix around the patch is enriched in Na, and Ep needles can be found in the vicinity of this patch (Figure 2a,c). There are also patches present that do not reveal the growth of new phases such as Qz and Ep, at least not in this two-dimensional view of the exposed sample surface (Figure 3).

The drill core sample G_2.5_900, deformed at 2.5 GPa and 900°C, exhibits extensive cracking, slip along cleavage cracks, and deformation twinning in plagioclase in plane and crossed polarized light (Figure 6a,b,g,h). At higher magnification, areas that consist of finely grained material become visible (Figure 6c,d,g,h). This fine-grained material appears to form two sets of parallel bands that are oriented almost perpendicular to each other (Figure 6c–f). Further, these parallel bands seem to preferentially form in the vicinity of narrow zones, appearing darker than the surrounding plagioclase in BSE mode (Figure 6e,j) and are often found along cleavage cracks (Figure 6g–j). The parallel bands are made of two different phases, which could not be identified unequivocally, because of the small grain size (Figure 6k). Strikingly, the orientation of these parallel bands, made of these two small phases, coincides with the orientation of deformation twins (Figure 6d,e,f,h,j). Similar to samples D_2.5_720-950 and G_2.5_700, demonstrating a close spatial relation between cracking, twinning, and the presence of new phases, the drill core samples also exhibit that reaction dominantly occurs in areas that underwent pronounced deformation (Figures 1, 5, and 6).

Sample P_3_950, which experienced hydrostatic conditions, demonstrates dark areas that are mostly located along grain and interphase boundaries (Figure 7a). Within these dark zones, new eclogite-facies phases grew

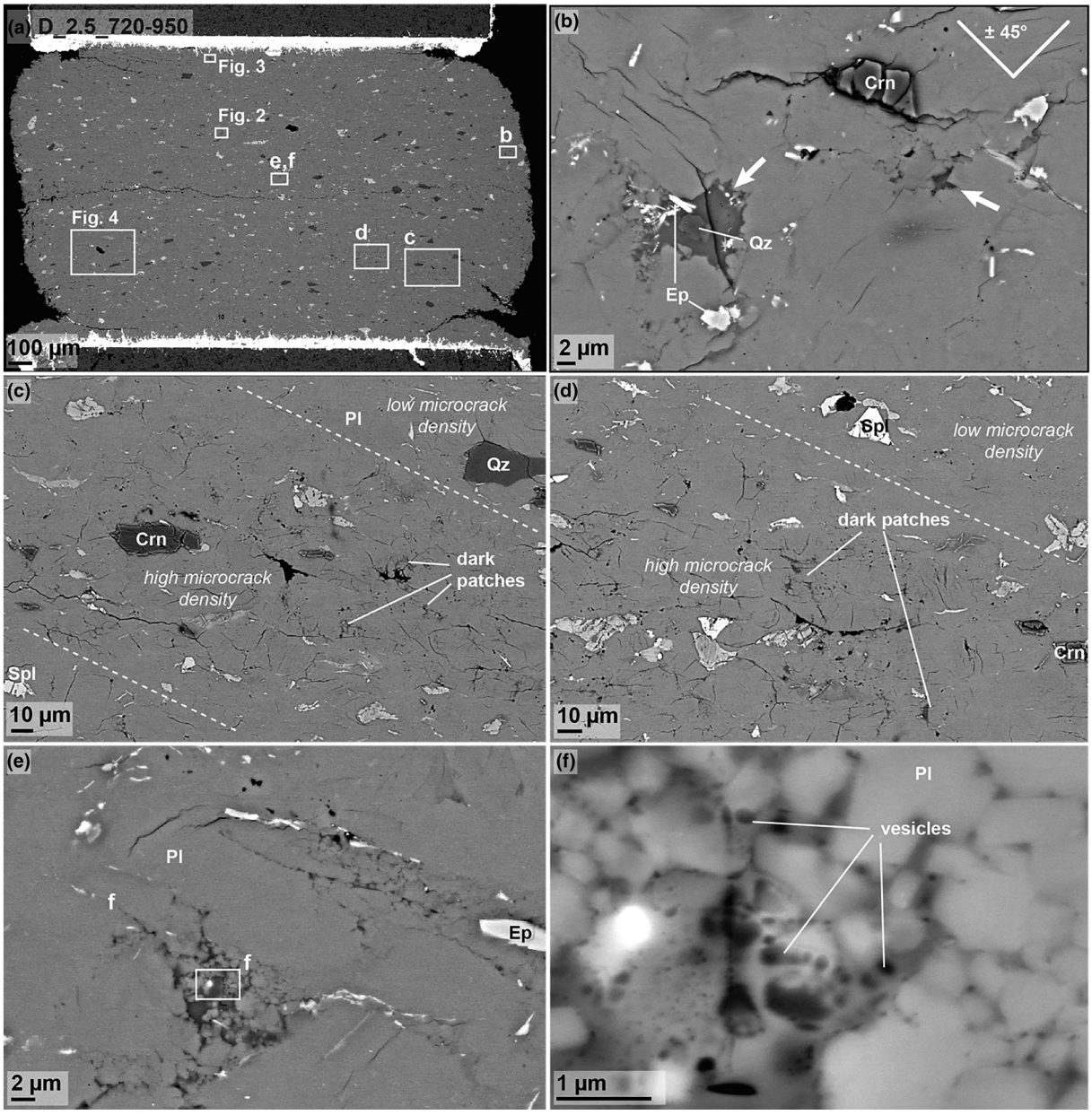

FIGURE 1 Backscatter electron images of the deformation multianvil apparatus sample D_2.5_720-950. (a) Low-magnification images of the sample with white rectangles marking the location of the Figures 2–4. (b) Dark patch with quartz and epidote grains. White arrows highlight another small patch that shows very sharp edges orientated with ±45° relative to σ_1 (perpendicular to the long edge of the image). (c, d) Dark patches mostly occur in areas with a high microcrack density limited by white dashed lines. (e) Some dark patches do not reveal any particular shape. (f) High-magnification image of the area marked in (e) showing numerous vesicles in the dark material that fills the patch

such as Ep, Qz, Grt, Omp, titanite (Ttn), and kyanite (Ky). Plagioclase twins are highlighted in red in the phase map shown in Figure 7b. Some plagioclase grains reveal parallel growth twin lamellae that run through the entire grain and a few lenticular-shaped deformation twins marked by red arrows in Figure 7b. In contrast to the deformation twins, found in the deformation samples, the deformation twins in the hydrostatic sample do not show a uniform orientation (Figure 7b). However, they show a close spatial relation with non-indexed areas of a few micrometre in size similar to the deformation twins in the deformation samples (red arrows in Figure 7b,c) in which we find bright, newly formed phases too small to be unequivocally identified (Figure 7a).

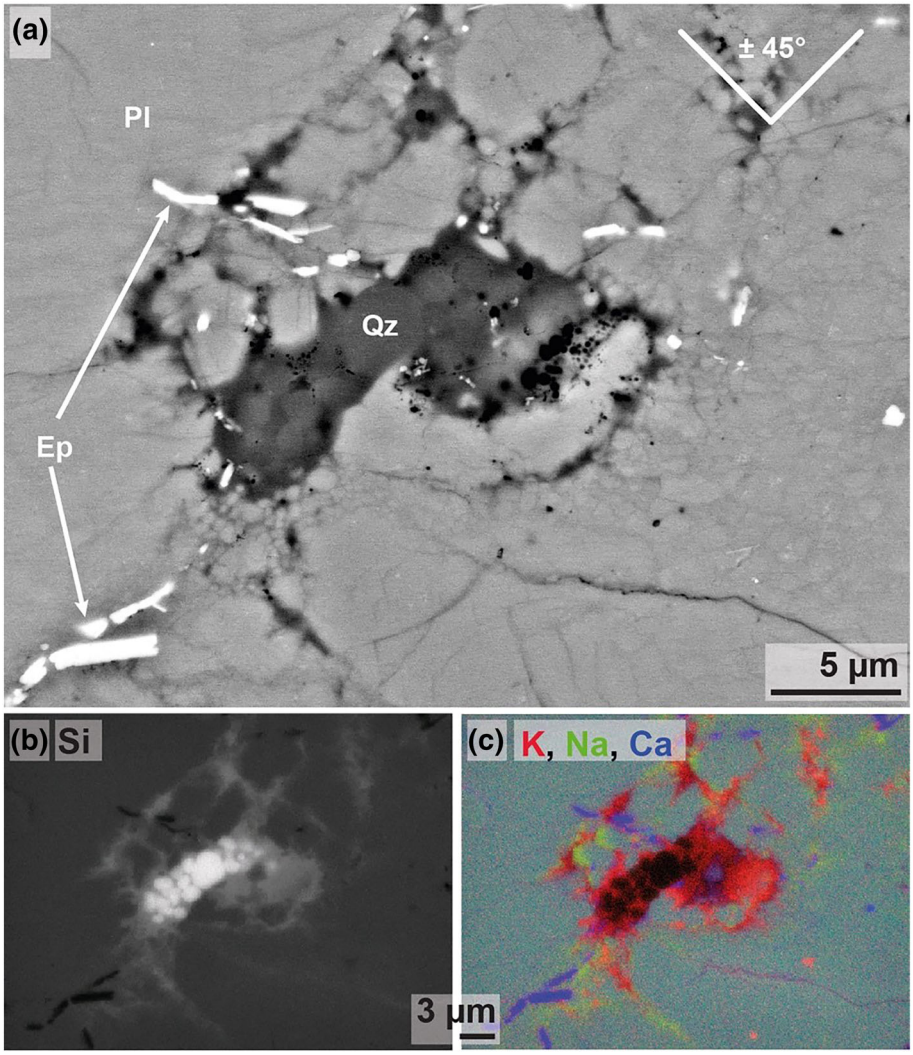

FIGURE 2 (a) High-magnification backscatter electron image showing a patch appearing darker than the surrounding plagioclase matrix. Subeuhedral quartz (Qz) formed within the patch and in its vicinity, we find needles of an epidote group mineral (Ep). The patch shows edges that are oriented at ±45° towards the direction of maximum compression (perpendicular to the long edge of the image). (b) Si-element distribution map of the area shown in (a) exhibiting that the patch filling material is enriched in Si. (c) Composite image of K-, Na-, and Ca-element distribution maps revealing that the patch filling material is enriched in K and the surrounding plagioclase is richer in Na relative to plagioclase from the starting material. Ep, epidote group mineral; Pl, plagioclase; Qz, quartz

4 | DISCUSSION

4.1 | Semibrittle deformation in plagioclase-rich rocks

In the deformation samples, we observe (i) a wide variation in grain size, indicative of cataclasis, that results from fracturing of grains unfavourably oriented for deformation twinning whereas favourably oriented plagioclase grains deformed by deformation twinning (Figure 4b), (ii) a close spatial relation between cleavage cracking and twinning (Figures 5 and 6), and (iii) slip along cleavage cracks adjacent to extensively twinned regions (Figure 6h). The association between brittle cracking and plastic deformation twinning clearly demonstrates that the deformation took place in the semibrittle regime. The seminal study by Tullis and Yund (1992) experimentally demonstrated that plagioclase-rich rocks deform by a mixture of brittle and plastic deformation mechanisms over a broad P–T–$\dot{\varepsilon}$ range. Previous studies discussed that brittle and plastic deformation often do not occur parallel but are strongly coupled and thus interdependent in plagioclase (McLaren & Pryer, 2001; Stünitz et al., 2003). This interplay between brittle microcracking and plastic deformation twinning is particularly clear at the grain scale in our deformation samples, in which we find deformation twins spatially associated with cleavage cracks (Figures 4b,c and 5). Deformation twins are often limited by {001} cleavage cracks (Figures 4b,c and 5), and we, therefore, interpret that the high stresses at the twin tips caused microcracking along {001} to relieve the stress and to stabilize or pin the twin (McLaren & Pryer, 2001). Yet, another possible scenario could be that cracking preceded twinning. Due to the high stresses at crack tips, the material affected will deform plastically in a zone around the crack tip thus called crack tip plastic zone. Crack formation will therefore produce zones with a high dislocation density in its vicinity, evidenced by transmission electron microscopy analyses in plagioclase Figure 5a in Stünitz et al. (2003). Hence, plastic deformation can nucleate in areas that underwent brittle deformation (McLaren & Pryer, 2001). Regardless of the exact deformation

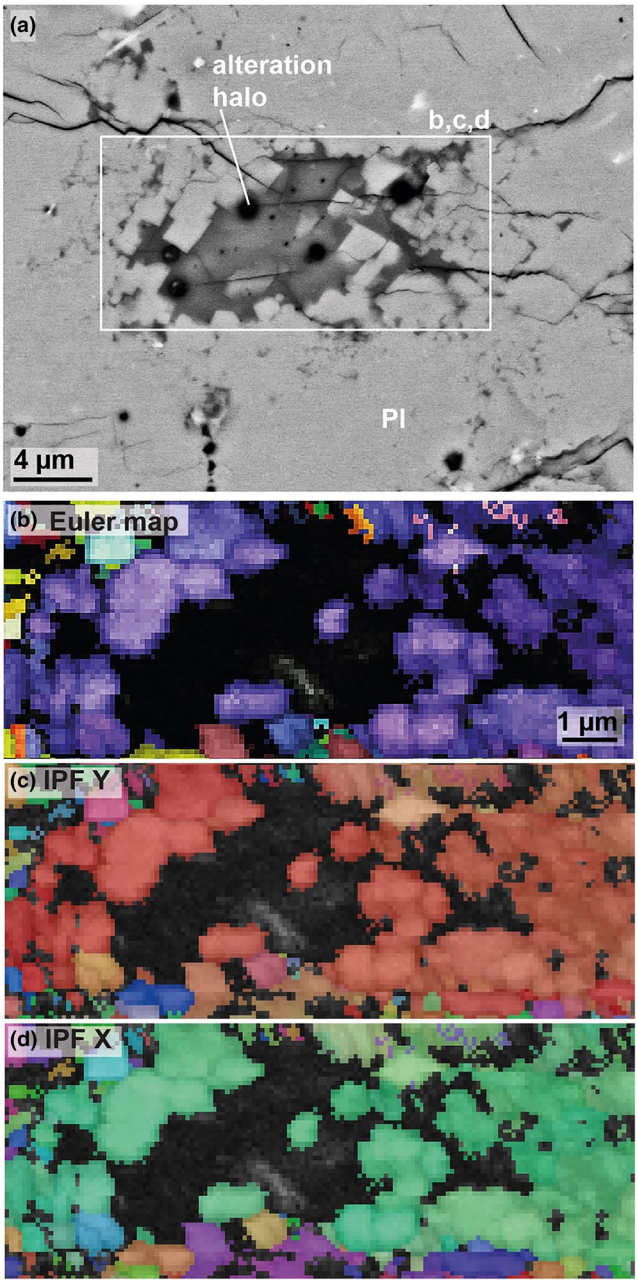

FIGURE 3 (a) Microstructural data of a patch appearing darker relative to the surrounding plagioclase matrix in backscatter electron mode. (b–d) Euler map and inverse pole figure (IPFs) of the area marked in (a). The non-indexed areas are shown in black. Most of the grains surrounding the patch show no or very little difference in grain orientation.

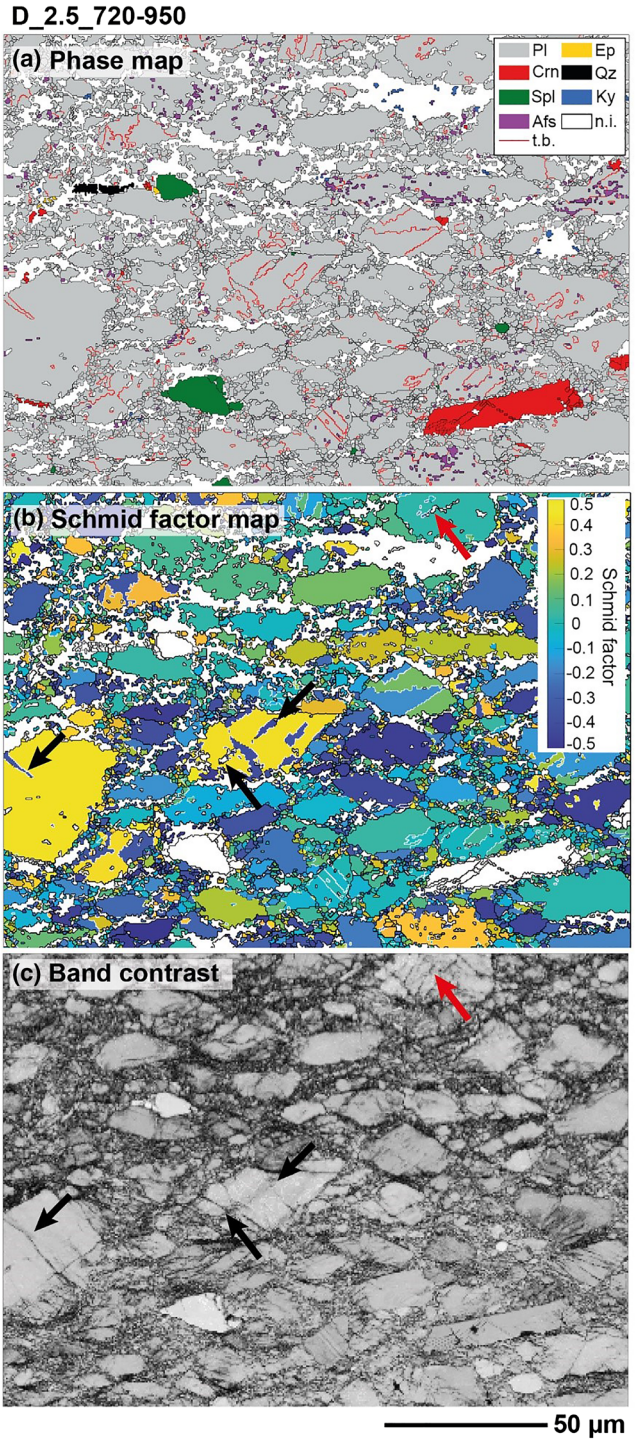

FIGURE 4 Electron-backscatter diffraction data of the area marked in Figure 1. (a) Phase map showing the growth of new phases and the location of non-indexed areas. (b) Schmid factor map. Black arrows highlight the deformation twins that were favourably oriented for deformation twinning. (c) Band contrast image showing that plagioclase grains that underwent deformation twinning also reveal numerous microcracks. Afs, alkali-feldspar; Crn, corundum; Ep, epidote group mineral; Ky, kyanite; n.i., not indexed; Pl, plagioclase; Qz, quartz; Spl, spinel; t.b., twin boundary

sequence, both processes, cracking and deformation twinning, will locally increase the dislocation density, and stress relief will result in the creation of new interfaces, for example, cleavage cracks or cracks in general and twin boundaries.

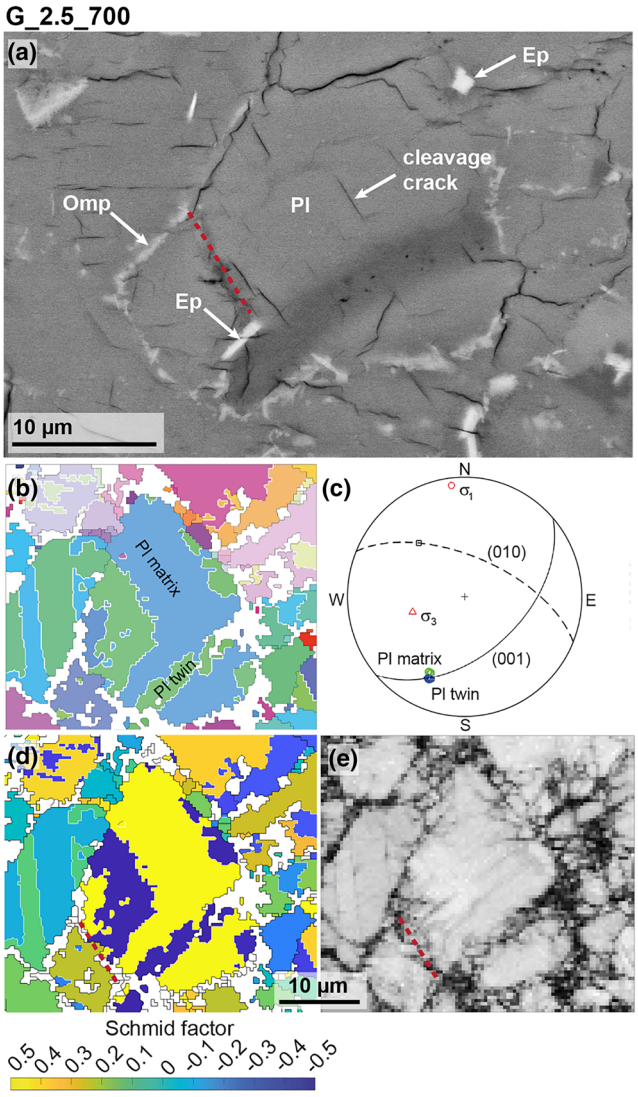

FIGURE 5 Microstructural analyses of the Griggs deformation sample G_2.5_700 that experienced deformation at a strain rate of $4{\cdot}10^{-6}$ s^{-1} under 2.5 GPa and 700°C. The red dashed line was added as marker to facilitate the comparison between the images. The direction of maximum compression (σ_1) is oriented perpendicular to the upper and bottom edges of the images. (a) Backscatter electron image showing a plagioclase grain with numerous cleavage cracks surrounded by mainly Omp and Ep. Latter also form euhedral grains. (b, c) Inverse pole figure and corresponding stereonet showing the orientation of the Pl matrix and Pl twin. (d) Schmid factor map exhibiting that the band, appearing dark in backscatter electron mode in (a), follows a deformation twin in plagioclase and is sensitive to the electron beam indicated by the formation of alteration holes. (e) Band contrast image demonstrating that twins are spatially associated with cracks. Ep, epidote group mineral; Omp, omphacite; Pl, plagioclase

4.2 | Partial melting of plagioclase

We found zones made of a material, which contains vesicles and is sensitive to the electron beam (Figures 1–3, and 5), and sometimes hosts subhedral or euhedral Qz and/or Ep grains (Figures 1b, 2b, and 5a), all indicators that partial melting took place. Furthermore, the chemical composition of the patches demonstrates enrichment in Si and K relative to the initial plagioclase composition (Figure 2b,c). This particular chemical signature has been previously observed in partially molten plagioclase samples (Dimanov et al., 2000; Tsuchiyama & Takahashi, 1983) and in natural shock molten plagioclase (Chen & El Goresy, 2000) and also fits the expected melt composition calculated using Perple_X. Thermodynamic calculations also demonstrate that partial melting occurs beyond ~810°C at 2.5 GPa and above ~900°C at 3 GPa (Figure 8). The extent of melting, found in the samples, correlates with the maximum temperature reached and the time the samples spent at that temperature. Drill-core sample G_2.5_900 shows a similar amount of partial melting relative to the DDIA sample that experienced up to 950°C, and both samples show less melting relative to the static sample P_3_950 that remained at 950°C for 24 h. Yet, it is difficult to directly compare the amount of melting observed in samples in which we used powders with those in which we used a drill core due to the large difference in grain size (<38 vs. ~1000 µm). The reason we observe a similar amount of partial melting in the drill core sample G_2.5_900 and the DDIA sample D_2.5_720-900 is probably the result of a counterbalancing effect on melting kinetics between grain size and time spent at high temperatures. Although the drill core sample has a much larger grains size, which is ~2 orders of magnitude larger relative to the DDIA sample, it spent with ~1.6 h around twice the time at 900°C than the DDIA sample that experienced temperatures of 900 to 950°C for only 0.75 h.

The thermodynamic calculations show that sample G_2.5_700 should not undergo partial melting. The presence of areas with a small grain size (<1 µm) that consequently show a high crack density could also produce non-indexation in EBSD data. Extreme grain size reduction or grain comminution have been previously documented in samples that experienced large displacements (Pec et al., 2012; Yund et al., 1990). The absence of large displacements in the microstructures of these samples (Figure 5b), however, as well as the lack of significant differences in grain orientation (Figure 5b) of the surrounding plagioclase, eliminates grain comminution as cause of the formation of these non-indexed zones. Combining various microstructural data of these samples reveals that deformation twins are spatially associated with grain-scale microcracks (Figure 5). Therefore, the interplay between plastic deformation twinning and brittle cracking at the grain scale may result in an extensively twinned and cracked volume. Although we do not have

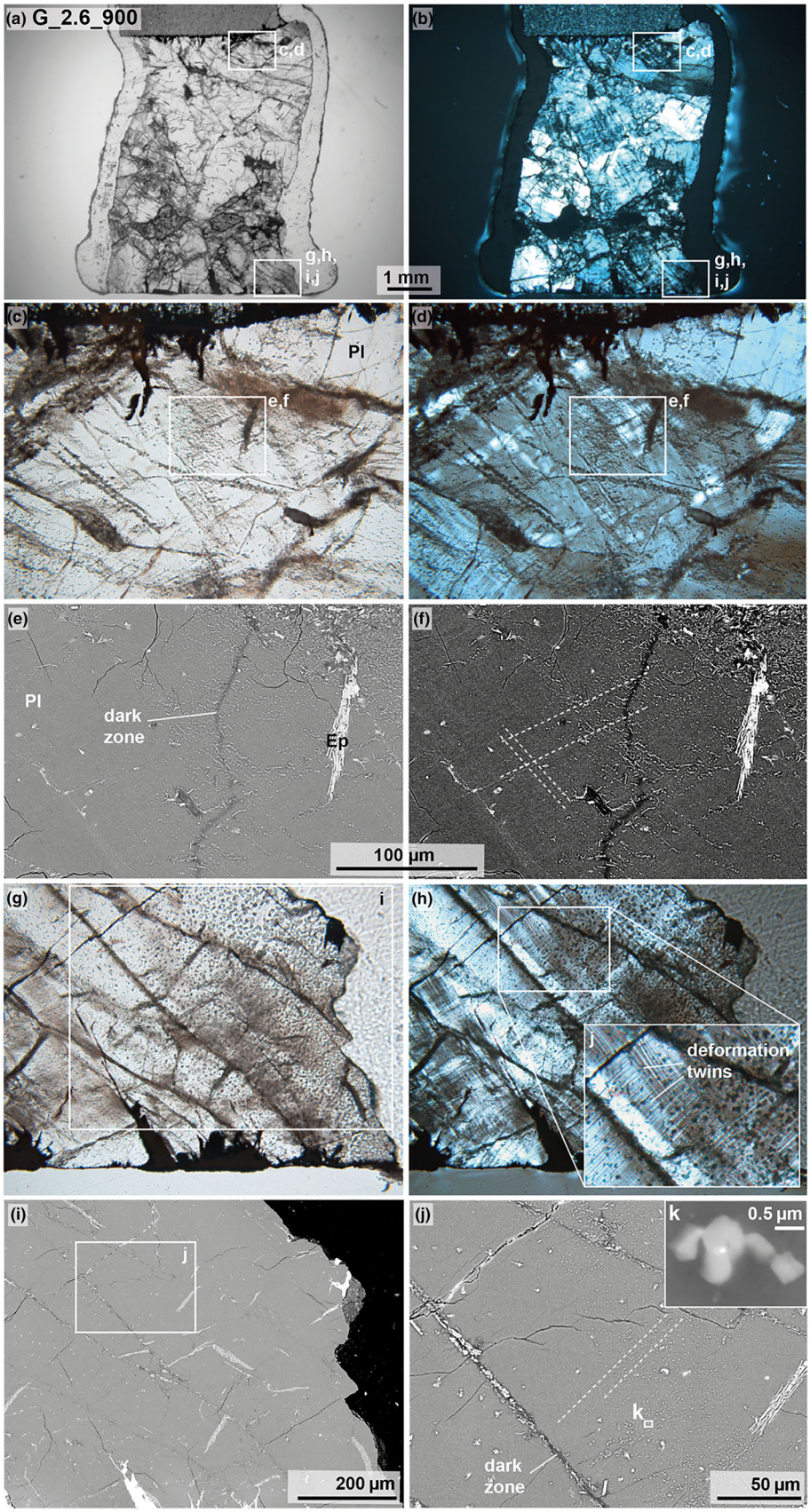

FIGURE 6 Drill core sample G_2.5_900 deformed in a Griggs press at 2.5 GPa, 900°C to ~35% axial strain. Image taken (a) in plane polarized light and (b) in crossed polarized light marking the locations for the high-magnification images presented in (c), (d), (g), and (h). (c, d) Area with small grains visible in plane polarized light (c) that coincides with the occurrence of deformation twins visible in crossed polarized light (d). (e, f) Backscatter electron images of the areas marked in (c) and (d) exhibiting two sets of planes that are formed by tiny, bright phases. These bright phases mainly formed in the vicinity of the dark appearing vein. (g, h) Extensive cleavage cracking in the lower right corner of the sample shown in plane and crossed polarized light. (i, j) The cracks are filled with a dark material in which bright phases grew identified as Ep. In the vicinity of the cracks, we find parallel planes that are made of these bright phases. A high-magnification image of these phases is presented in (k).

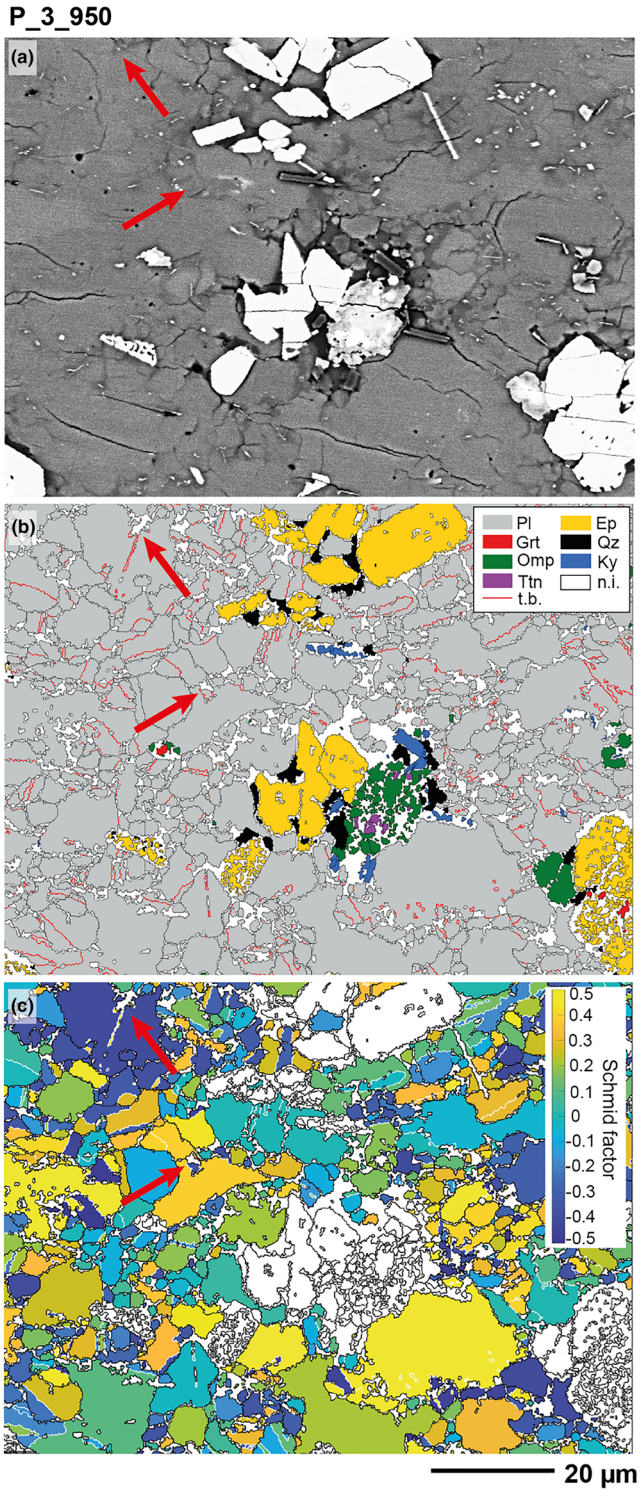

FIGURE 7 Microstructural analyses of the hydrostatic sample P_2.5_950 that experienced 3 GPa and 950°C for 24 h in backscatter electron mode (a), as phase map (b), and as Schmid factor map (c). The red arrows in (b) and (c) mark the position of deformation twins associated with non-indexed zones. Ep, epidote group mineral; Grt, garnet; i.n., not indexed; Ky, kyanite; Omp, omphacite; Pl, plagioclase; Qz, quartz; t.b., twin boundary; Ttn, titanite/sphene

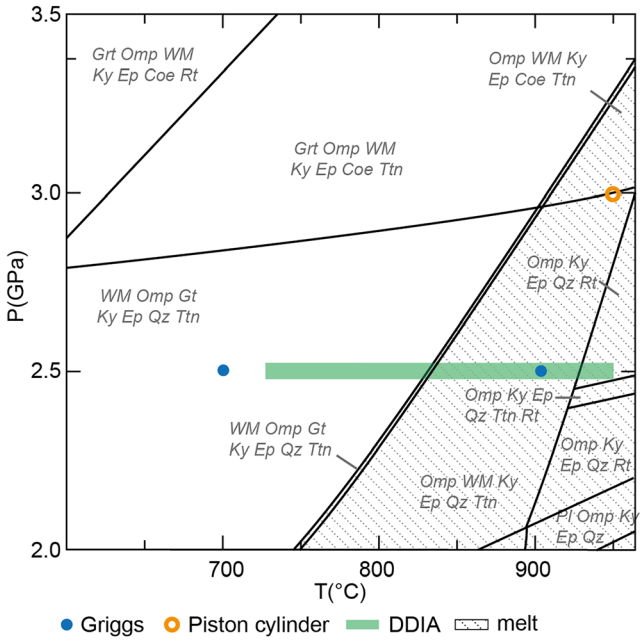

FIGURE 8 *P–T* pseudosection showing the expected onset of melting in the samples at elevated temperatures (dashed area). Coe, coesite; Ep, epidote-group mineral; Ky, kyanite; Omp, omphacite; Pl, plagioclase; Qz, quartz; Rt, rutile; Ttn, titanite/sphene; WM, white mica

unequivocal evidence that melting occurred in this region, the sensitivity to the electron beam as evidenced by alteration haloes and the growth of euhedral Ep suggest that partial melting took place locally.

4.3 | Nucleation sites for melt and melt initiation

We observe that melting and reaction occurred in two different sites. One site was along grain or interphase boundaries resulting in zones with no particular shape (Figures 1c–e, 4a,b, 5b, and 7). A second melting and reaction site is restricted to deformation features such as cracks and/or deformation twins. Sample G_2.5_900 clearly displays the occurrence of melting along cracks and cleavage cracks (Figure 6e,j). EBSD data demonstrate the close spatial relation between deformation twins spatially associated with cracks and zones that we interpret as quenched partial melt for the above-mentioned reasons of being sensitive to the electron beam, containing vesicles, exhibiting newly formed subhedral or euhedral grains, and showing non-indexation in EBSD data (Figures 1b,f, 2a, 3a, 4b, and 5b).

In order to initialize melting of a solid, the interfacial energy between melt and solid must be overcome.

Further, melting temperatures are typically dramatically decreased in the presence of water (Johannes et al., 1994). Partial melting is expected to initiate at grain or interphase boundaries, cracks, and cleavage planes, because these loci show higher interface energies than the intact grain interior (Tsuchiyama & Takahashi, 1983) and because that is where fluids can more easily percolate, further lowering the melting point. Apart from the influence of H_2O on decreasing melting temperatures, it has been shown that the presence of SiO_2 either from an external SiO_2 source such as quartz or due to plagioclase decomposition itself (albite $\leftrightarrow$ jadeite + quartz; Holland, 1980) further lowers the melting point of plagioclase if an Al_2O_3 sink is present (Johannes et al., 1994). In sample D_2.5_720-950, we observe a clear enrichment of SiO_2 in the melt patches due to the decomposition of plagioclase and find epidote grains that can act as Al_2O_3 sink before kyanite starts to nucleate and grow at a reaction progress above ~10% (Figures 1c and 3a; Wayte et al., 1989). The enrichment in Si in the melt patches eventually caused the growth of quartz. Some melt patches appear to lack new crystallites (Figure 1d), because (i) they are simply not exposed on the surface or (ii) partial melting did not occur at the same time throughout the sample and those patches lacking quartz crystals represent partial melting that took place at a later stage during deformation. As a result, the crystals had insufficient time to nucleate and grow prior to quenching. Melt patches showing quartz grains uniformly exhibit rougher patch edges (Figures 1b and 2) relative to those that lack quartz and show very smooth edges (Figure 3). The roughness is probably due to ongoing deformation causing further grain size reduction and grain rotation, therefore destroying the sharpness of the initial patch edges. This scenario would thus support the hypothesis that patches lacking quartz formed at a later stage during deformation, and therefore, the pristine melting structure is still preserved.

Johannes et al. (1994) experimentally demonstrated that wet melting mainly takes place along grain boundary and cracks, connected to the grain boundary, relative to dry melting that also affects the inside of plagioclase grains, for example, twin boundaries. This is well in accordance with our static sample, in which we mainly observe melting along plagioclase grain boundaries evidenced by melt patches showing no particular orientation (Figure 4). Yet, in addition to reaction and partial melting along grain boundaries, the samples also exhibit melting along cracks and deformation twin boundaries and thus of the grain interiors, which has solely been observed for dry partial melting of plagioclase >1300°C (Figures 1–3; Johannes et al., 1994, Tsuchiyama & Takahashi, 1983).

4.4 | Deformation-facilitated melting and reaction

In contrast to growth twins, deformation twins show considerable distortion of the material in their vicinity (Cahn, 1954, ch. 3.1.8, p. 420), which is accommodated by twinning disconnections (Hirth et al., 2019; Xie et al., 2019), resulting in higher interface energies relative to areas around parallel sided, through-going growth twins (Brown & Macaudière, 1986) or along deformation twin boundaries that underwent recovery. Thus, the highly strained areas around the lenticular-shaped deformation twins represent higher internal energy domains where the energy threshold for melting reactions could be more easily overcome. It has also been demonstrated in previous studies that deformation twins are prone to chemical etching (Cahn, 1954, ch. 3.1.8, p. 420) as well as to partial melting at dry experimental conditions > 1100°C (Johannes et al., 1994; Tsuchiyama & Takahashi, 1983), and the isotropization along twin boundaries is also used to estimate conditions during shock metamorphism (Bischoff & Stöffler, 1992).

Although melting could be facilitated due to a higher defect density associated with deformation twins, the maximum temperatures during deformation did not surpass 950°C and thus remained 375°C to 625°C below plagioclase's dry solidus of 1325°C. However, it is likely that during sample preparation of the powdered samples, water from air humidity adhered onto the grain surfaces, supported by the observation that most Ep formed along plagioclase grains (Figure 5). Deformation twins are either limited by grain boundaries or cracks connected to the grain boundary and are thus either directly or indirectly connected with the wetted grain boundaries (Figures 4 and 5). In addition to melting along grain boundaries, we, therefore, observe melting along deformation twins that either directly commence at grain boundaries or are linked to grain boundaries via cracks providing a fluid pathway into the grain's interior (Figure 5b).

Because grains that show growth twins did not undergo partial melting, it appears that the combination of the high defect density around deformation twins associated with cracks in conjunction with minor amounts of fluid leads to partial melting inside of deformed plagioclase grains. Strikingly, the presence of non-indexed areas along deformation twins in the piston-cylinder sample provides evidence that partial melting along deformation twin boundaries also occurred under hydrostatic conditions (red arrows in Figure 7b,c). Some of these deformation twins were probably already present in the starting material or local stress concentration due to volume changes during reaction of the sample caused deformation twinning and subsequent melting in plagioclase during

the test. Regardless of the formation history of these deformation twins, they are likely to be surrounded by a higher defect concentration than an undeformed area within plagioclase. Defect-facilitated melting could also explain the occurrence of partial melting in sample G_2.5_700, in which thermodynamic modelling does not predict partial melting at 2.5 GPa and 700°C (Figures 5 and 8).

A previous study documented partial melting in perthite samples deformed in the semibrittle regime (Negrini et al., 2014). The authors observe melting to be restricted to areas that underwent extensive microcracking and therefore conclude that the initiation of melting is likely to be caused by dilatancy during cracking. Because we also find that melting in the deformation samples is spatially associated with areas exhibiting a high microcrack density (Figure 1), melting due to dilatancy caused by cracking is also a viable explanation in our samples. In addition to melting caused by cracking, we also document that deformation twinning or rather the interdependence between deformation twinning and cracking can cause melting even inside of plagioclase grains. The preferential growth of the plagioclase decomposition phases Ep and Omp in parallel planes that coincide with deformation twins (Figure 6e,j) also demonstrates that reaction in general is not limited to grain or interphase boundaries but affects other intragrain interfaces such as cleavage cracks and deformation twin boundaries. To summarize, our study and previous studies on plagioclase deformation demonstrate that deformation twinning and cracking are interdependent (McLaren & Pryer, 2001; Tullis & Yund, 1992). Because both mechanisms are so closely spatially related, it is difficult to determine if cracking and accompanied dilatancy led to melting, as demonstrated by Negrini et al. (2014), or if the local increase in defect density due to the interplay between cracking and deformation twinning facilitated partial melting and reaction. Most likely partial melting in our samples is a result of both processes—melt initiation due to dilatancy caused by cracking (Figure 1) and the onset of melting due the interaction between deformation twins and cracks resulting in a higher defect density (e.g., Figure 5).

4.5 | Link to nature

In general, natural long-term deformation rates are ~7 orders of magnitudes slower than our laboratory strain rates. However, deformation twinning mainly depends on stress magnitude and stress direction and is rather insensitive to variations in strain rate (Borg & Handin, 1966; Borg & Heard, 1969; De Bresser & Spiers, 1990, 1997; Rowe & Rutter, 1990). Furthermore, due to the presence of one perfect and one good cleavage plane in plagioclase, cleavage cracking is likely to prevail even at lower strain rates.

It is expected that plagioclase-rich rocks of the lower continental crust equilibrated at granulite-facies conditions corresponding to temperatures of 800°C to 900°C and pressures below 1 GPa (Austrheim & Griffin, 1985). Therefore, partial melting, starting at temperatures >750°C and pressures >1 GPa, is not expected under granulite-facies conditions (Boettcher, 1970; Goldsmith, 1981). Yet, in an anisotropic stress field, the maximum principal stress (σ_1) could be locally much higher, for example, at grain–grain contacts, thus surpassing plagioclase's wet solidus (Hirth & Tullis, 1994; Kirby, 1987; Richter et al., 2016). Lower crustal rocks exposed throughout Norway (Bergen Arcs, Western Gneiss Region, and Lofoten archipelago) indicate peak pressure at eclogite-facies peak-pressure conditions (Austrheim & Griffin, 1985; Bhowany et al., 2017; John et al., 2009; Steltenpohl et al., 2006). The exact timing of peak temperature and peak pressure conditions a rock mass experienced are often difficult to constrain. Therefore, during ongoing crustal thickening, it is possible that the rock masses cross the wet solidus thus tracing an anticlockwise *P*–*T* path, which has been discussed for the Scandinavian Caledonides (Faber et al., 2019). Previous studies also documented and discussed the occurrence of partial melts in plagioclase-rich rocks that formed at UHP conditions (Labrousse et al., 2011; Vrijmoed et al., 2009). Deformation-facilitated partial melting of plagioclase along deformation features such as deformation twins and cleavage cracks would therefore be relevant for settings in which the continental crust has been thickened due to continent collision, for example, the Himalayas and the Scandinavian Caledonides, and especially in the deep continental crust close to the Mohorovičić discontinuity where pressures and temperatures are the highest.

Furthermore, shearing associated with twinning under high differential stresses and temperatures could also contribute to local shear heating, especially because twinning occurs very rapidly as evidenced by acoustic emissions in laboratory experiments on various metals (e.g., Christian & Mahajan, 1995, p. 147). A local temperature increase ΔT due to plastic shearing can be expressed by

$$\Delta T = (\sigma_d \cdot \gamma)/(\rho \cdot c_p). \quad (1)$$

The shear strain γ associated with twinning in plagioclase is 0.136 (Borg & Handin, 1966; Xie et al., 2019). Using the inverted Schmid's law

$$\sigma_1 - \sigma_3 = \sigma_{CRSS}/(\cos(\gamma)\cos(\theta) \quad (2)$$

and a critical resolved shear stress σ_{CRSS} of 100 MPa for albite twinning (0.8 to 1.0 GPa at 800°C; estimated by Borg & Heard, 1969) would give a differential stress (σ_1-σ_3) of 0.2 GPa if the crystal was ideally oriented for twinning, that is, cos(γ)cos(θ) = 0.5, where γ is the angle of the normal to the glide or in this case twin plane with the maximum principal stress and θ is the angle between the maximum compression direction and the glide direction. Taking 0.2 GPa as lower bound for the differential stress estimate and 0.8 GPa as upper bound (Tajčmanová et al., 2014), a specific heat capacity for plagioclase of $c_p = 907\ J\ kg^{-1}\ K^{-1}$ (Benisek et al., 2009) and a plagioclase density ρ of 2760 kg cm^{-3} (Hacker et al., 2003) would lead to an increase in temperature ΔT of ~10°C to 40°C. Yet, transient stresses caused by seismic events might be much higher as evidenced by pulverized garnet grains in natural and experimental rocks (Austrheim et al., 2017; Incel, Schubnel, et al., 2019). Experimental data on plagioclase aggregates, deformed under H*P*, high-temperature conditions (2.5–3 GPa and 720–950°C), demonstrate differential stresses of up to 2 to 3 GPa (Incel, Labrousse, et al., 2019), and sample G_2.5_700 experienced a maximum differential stress of ~1.5 GPa. However, due to the sample geometry as well as due to grain–grain contacts, stresses may have been locally much higher. These high differential stresses would lead to a twin-induced temperature increase of ~110°C to 160°C and of ~80°C for sample G_2.5_700. Considering an error for the temperature of ~20°C together with the uncertainty of modelling partial melting using thermodynamic databases, a temperature increase of 80°C due to twinning shear in conjunction with a high defect density may have caused partial melting along deformation twins in sample G_2.5_700. Thus, under high stresses in the GPa range due to elevated deformation rates, twinning shear could initiate local melting at background temperatures significantly lower than the melting point. This is especially interesting for situations in which dry and therefore strong plagioclase-rich rocks survive metastable at H*P* high temperature conditions of the eclogite-facies (Austrheim & Griffin, 1985; Stünitz & Tullis, 2001; Tullis & Yund, 1992).

5 | CONCLUSION AND IMPLICATIONS

In the present experimental study, we performed a hydrostatic experiment in a piston-cylinder press and several deformation tests in three different deformation apparatus, a DDIA apparatus and two Griggs presses, on granulite samples under eclogite-facies conditions. In every sample, we observed evidence for partial melting due to the decomposition of plagioclase at H*P*, high-temperature conditions in the presence of H_2O. Deformation features such as deformation twins spatially related with cleavage cracks or cracks in general are additional sites for melt nucleation probably due to the high defect density associated with these deformation structures, but dilatancy due to cracking may also play a significant role in the initiation of melting (Negrini et al., 2014). Regardless of the underlying mechanism leading to melting (cracking or deformation twinning), the present study highlights a close coupling between deformation and melting/reaction. The exploitation of other crystallographic planes such as cleavage planes and deformation twins for melting and reaction in plagioclase may significantly decrease the sample grain size. Consequently, the lowered effective grain size will not only influence the deformation behaviour but also the reactivity of the sample. The occurrence of deformation twinning and associated reaction or even partial melting under eclogite-facies conditions could be one more process explaining the dramatic mechanical impact of eclogitization. This could add to the acknowledged transient weakening associated to eclogite formation (Stünitz et al., 2020), by promoting grain-size sensitive deformation mechanisms.

ACKNOWLEDGEMENTS

The authors want to thank the handling editor Katy Evans and the two reviewers, Jun Muto and Holger Stünitz, for their thorough reviews that helped improving this manuscript and especially thank Holger Stünitz for additional discussions. S. I. is very grateful to Marieke Rempe for the fruitful discussions during coffee breaks and walks, to Jörg Renner and Ralf Dohmen for helpful comments on the experimental results, and to Christopher Beyer for discussions on crystal melting. S. I. thanks Damien Deldicque for the EBSD analyses performed at ENS Paris. S. I. and A. S. thank Yanbin Wang, Nadège Hilairet, and Julien Gasc very much for their help during the experiments, and M. B. thanks Julien Siebert and Nicolas Wehr from the Institut de Physique du Globe Paris for the support during the piston-cylinder experiments. S. I. acknowledges the Alexander von Humboldt-foundation for funding her Humboldt fellowship. A. S. acknowledges the European Research Council grant REALISM (2016-grant 681346).

CONFLICT OF INTEREST

There is no conflict of interest.

ORCID

Marie Baïsset https://orcid.org/0000-0001-5611-5470

REFERENCES

Austrheim, H. (1986). Eclogitization of lower crustal granulites by fluid migration through shear zones. *Earth and Planetary Science Letters*, *81*, 221–232. https://doi.org/10.1016/0012-821X(87)90158-0

Austrheim, H., Dunkel, K. G., Plümper, O., Ildefonse, B., Liu, Y., & Jamtveit, B. (2017). Fragmentation of wall rock garnets during deep crustal earthquakes. *Science Advances*, *3*(2), 1–7. https://doi.org/10.1126/sciadv.1602067

Austrheim, H., & Griffin, W. L. (1985). Shear deformation and eclogite formation within granulite-facies anorthosites of the Bergen arcs, western Norway. *Chemical Geology*, *50*(1–3), 267–281. https://doi.org/10.1016/0009-2541(85)90124-X

Bachmann, F., Hielscher, R., & Schaeben, H. (2010). Texture analysis with MTEX—Free and open source software toolbox. *Solid State Phenomena*, *160*, 63–68. https://doi.org/10.4028/www.scientific.net/SSP.160.63

Benisek, A., Dachs, E., & Kroll, H. (2009). Excess heat capacity and entropy of mixing in high structural state plagioclase. *American Mineralogist*, *94*(8–9), 1153–1161. https://doi.org/10.2138/am.2009.3151

Bhowany, K., Hand, M., Clark, C., Kelsey, D. E., Reddy, S. M., Pearce, M. A., Tucker, N. M., & Morrissey, L. J. (2017). Phase equilibria modelling constraints on *P–T* conditions during fluid catalysed conversion of granulite to eclogite in the Bergen arcs, Norway. *Journal of Metamorphic Geology*, *36*(3), 315–342. https://doi.org/10.1111/jmg.12294

Bischoff, A., & Stöffler, D. (1992). Shock metamorphism as a fundamental process in the evolution of planetary bodies: Information from meteorites. *European Journal of Mineralogy*, *4*, 707–755. https://doi.org/10.1127/ejm/4/4/0707

Boettcher, A. L. (1970). The system CaO-Al_2O_3-SiO_2-H_2O at high pressures and temperatures. *Journal of Petrology*, *11*(69), 337–379. https://doi.org/10.1093/petrology/11.2.337

Borg, I., & Handin, J. (1966). Experimental deformation of crystalline rocks. *Tectonophysics*, *3*(4), 249–367. https://doi.org/10.1016/0040-1951(66)90019-9

Borg, I. Y., & Heard, H. C. (1969). Mechanical twinning and slip in experimentally deformed plagioclases. *Contributions to Mineralogy and Petrology*, *23*(2), 128–135. https://doi.org/10.1007/BF00375174

Brown, W. L., & Macaudière, J. (1986). Mechanical twinning of plagioclase in a deformed meta-anorthosite—The production of M-twinning. *Contributions to Mineralogy and Petrology*, *92*(1), 44–56. https://doi.org/10.1007/BF00373962

Cahn, R. W. (1954). Twinned crystals. *Advances in Physics*, *3*(12), 363–445. https://doi.org/10.1080/00018735400101223

Cao, Y., Liu, L., Yang, W., Gao, Y., & Zhu, X. (2019). Reconstruction the process of partial melting of the retrograde eclogite from the North Qaidam, Western China: Constraints from Titanite U-Pb dating and mineral chemistry. *Journal of Earth Science*, *30*(6), 1166–1177. https://doi.org/10.1007/s12583-019-1253-6

Chen, M., & El Goresy, A. (2000). The nature of maskelynite in shocked meteorites: Not diaplectic glass but a glass quenched from shock-induced dense melt at high pressures. *Earth and Planetary Science Letters*, *179*(3–4), 489–502. https://doi.org/10.1016/S0012-821X(00)00130-8

Christian, J. W., & Mahajan, S. (1995). Deformation twinning. *Progress in Materials Science*, *39*, 1–157. https://doi.org/10.1016/0079-6425(94)00007-7

Connolly, J. A. D. (1990). Multivariable phase diagrams: An algorithm based on generalized thermodynamics. *American Journal of Science*, *290*, 666–718. https://doi.org/10.2475/ajs.290.6.666

De Bresser, J. H. P., & Spiers, C. J. (1990). High-temperature deformation of calcite single crystals by r^+ and f^+ slip. In R. J. Knipe & E. H. Rutter (Eds.). *Geological society special publication* (Vol. 54) (pp. 285–298). Geological Society Special Publications. https://doi.org/10.1144/GSL.SP.1990.054.01.25

De Bresser, J. H. P., & Spiers, C. J. (1997). Strength characteristics of the r, f, and c slip systems in calcite. *Tectonophysics*, *272*(1), 1–23. https://doi.org/10.1016/S0040-1951(96)00273-9

Dimanov, A., Wirth, R., & Dresen, G. (2000). The effect of melt distribution on the rheology of plagioclase rocks. *Tectonophysics*, *328*(3–4), 307–327. https://doi.org/10.1016/S0040-1951(00)00214-6

Faber, C., Stünitz, H., Gasser, D., Jeřábek, P., Kraus, K., Corfu, F., Ravna, E. K., & Konopásek, J. (2019). Anticlockwise metamorphic pressure-temperature paths and nappe stacking in the Reisa Nappe Complex in the Scandinavian Caledonides, northern Norway: Evidence for weakening of lower continental crust before and during continental collision. *Solid Earth*, *10*(1), 117–148. https://doi.org/10.5194/se-10-117-2019

Ferrero, S., Wunder, B., Walczak, K., O'Brien, P. J., & Ziemann, M. A. (2015). Preserved near ultrahigh-pressure melt from continental crust subducted to mantle depths. *Geology*, *43*, 447–450. https://doi.org/10.1130/G36534.1

Fukuda, J., Muto, J., Koizumi, S., Sawa, S., & Nagahama, H. (2022). Enhancement of ductile deformation in polycrystalline anorthite due to the addition of water. *Journal of Structural Geology*, *156*(February), 104547. https://doi.org/10.1016/j.jsg.2022.104547

Fukuda, J.-i., Muto, J., & Nagahama, H. (2018). Strain localization and fabric development in polycrystalline anorthite + melt by water diffusion in an axial deformation experiment. *Earth, Planets and Space*, *70*(1), 3. https://doi.org/10.1186/s40623-017-0776-2

Goldsmith, J. R. (1981). The join $CaAl_2Si_2O$–H_2O (anorthite–water) at elevated pressures and temperatures. *American Mineralogist*, *66*, 1183–1188.

Hacker, B. R., Abers, G. A., & Peacock, S. M. (2003). Subduction factory 1. Theoretical mineralogy, densities, seismic wave speeds, and H_2O contents. *Journal of Geophysical Research: Solid Earth*, *108*(B1), 1–26. https://doi.org/10.1029/2001JB001127

Hilairet, N., Wang, Y., Sanehira, T., Merkel, S., & Mei, S. (2012). Deformation of olivine under mantle conditions: An in situ high-pressure, high-temperature study using monochromatic synchrotron radiation. *Journal of Geophysical Research: Solid Earth*, *117*(1), 1–16. https://doi.org/10.1029/2011JB008498

Hirth, G., & Tullis, J. (1992). Dislocation creep regimes in quartz aggregates. *Journal of Structural Geology*, *14*, 145–159. https://doi.org/10.1016/0191-8141(92)90053-Y

Hirth, G., & Tullis, J. (1994). The brittle-plastic transition in experimentally deformed quartz aggregates. *Journal of Geophysical Research: Solid Earth*, *99*(B6), 11731–11747. https://doi.org/10.1029/93JB02873

Hirth, J. P., Wang, J., & Hirth, G. (2019). A topological model for defects and interfaces in complex crystal structures. *American Mineralogist*, *104*(7), 966–972. https://doi.org/10.2138/am-2019-6892

Holland, T., & Powell, R. (1996). Thermodynamics of order-disorder in minerals: II. Symmetric formalism applied to solid solutions. *American Mineralogist*, *81*, 1425–1437. https://doi.org/10.2138/am-1996-11-1215

Holland, T., & Powell, R. (2003). Activity–composition relations for phases in petrological calculations: An asymmetric multicomponent formulation. *Contributions to Mineralogy and Petrology*, *145*, 492–501. https://doi.org/10.1007/s00410-003-0464-z

Holland, T. I. M., & Powell, R. (2001). Calculation of phase relations involving haplogranitic melts using an internally consistent thermodynamic dataset. *Journal of Petrology*, *42*(4), 673–683. https://doi.org/10.1093/petrology/42.4.673

Holland, T. J. B. (1980). The reaction albite = jadeite+quartz determined experimentally in the range 600–1200°C. *American Mineralogist*, *65*, 129–134. http://ammin.geoscienceworld.org/content/65/1-2/129.short

Holland, T. J. B., & Powell, R. (1998). An internally consistent thermodynamic data set for phases of petrological interest. *Journal of Metamorphic Geology*, *16*(3), 309–343. https://doi.org/10.1111/j.1525-1314.1998.00140.x

Incel, S., Hilairet, N., Labrousse, L., John, T., Deldicque, D., Ferrand, T. P., Wang, Y., Renner, J., Morales, L., & Schubnel, A. (2017). Laboratory earthquakes triggered during eclogitization of lawsonite-bearing blueschist. *Earth and Planetary Science Letters*, *459*, 320–331. https://doi.org/10.1016/j.epsl.2016.11.047

Incel, S., Labrousse, L., Hilairet, N., John, T., Gasc, J., Shi, F., Wang, Y., Andersen, T. B., Renard, F., Jamtveit, B., & Schubnel, A. (2019). Reaction-induced embrittlement of the lower continental crust. *Geology*, *47*(3), 235–238. https://doi.org/10.1130/G45527.1

Incel, S., Renner, J., & Jamtveit, B. (2020). Evolution of brittle structures in plagioclase-rich rocks at high-pressure and high-temperature conditions—Linking laboratory results to field observations. *Geochemistry, Geophysics, Geosystems*, *21*, 1–18. https://doi.org/10.1029/2020GC009028

Incel, S., Schubnel, A., Renner, J., John, T., Labrousse, L., Hilairet, N., Freeman, H., Wang, Y., Renard, F., & Jamtveit, B. (2019). Experimental evidence for wall-rock pulverization during dynamic rupture at ultra-high pressure conditions. *Earth and Planetary Science Letters*, *528*, 115832. https://doi.org/10.1016/j.epsl.2019.115832

Jamtveit, B., Putnis, C. V., & Malthe-Sørenssen, A. (2009). Reaction induced fracturing during replacement processes. *Contributions to Mineralogy and Petrology*, *157*(1), 127–133. https://doi.org/10.1007/s00410-008-0324-y

Johannes, W., Koepke, J., & Behrens, H. (1994). Partial melting reactions of plagciolase and plagioclase-bearing systems. In I. Parsons (Ed.). *Feldspars and their reactions* (pp. 161–194). Kluwer Academic Publishers. https://doi.org/10.1007/978-94-011-1106-5_4

John, T., Medvedev, S., Rüpke, L. H., Andersen, T. B., Podladchikov, Y. Y., & Austrheim, H. (2009). Generation of intermediate-depth earthquakes by self-localizing thermal runaway. *Nature Geoscience*, *2*(2), 137–140. https://doi.org/10.1038/ngeo419

John, T., & Schenk, V. (2003). Partial eclogitisation of gabbroic rocks in a late Precambrian subduction zone (Zambia): Prograde metamorphism triggered by fluid infiltration. *Contributions to Mineralogy and Petrology*, *146*, 174–191. https://doi.org/10.1007/s00410-003-0492-8

Kirby, S. H. (1987). Localized polymorphic phase transformations in high-pressure faults and applications to the physical mechanism of deep earthquakes. *Journal of Geophysical Research: Solid Earth*, *92*(B13), 13789–13800. https://doi.org/10.1029/JB092iB13p13789

Klein, C. (2001). *The 22nd edition of the manual of mineral science*. Wiley.

Labrousse, L., Prouteau, G., & Ganzhorn, A. C. (2011). Continental exhumation triggered by partial melting at ultrahigh pressure. *Geology*, *39*, 1171–1174. https://doi.org/10.1130/G32316.1

Marshall, D., & McLaren, A. (1977). Deformation mechanisms in experimentally deformed plagioclase feldspars. *Physics and Chemistry of Minerals*, *370*(August 1976), 351–370. https://doi.org/10.1007/BF00308845

McLaren, A. C., & Pryer, L. L. (2001). Microstructural investigation of the interaction and interdependence of cataclastic and plastic mechanisms in feldspar crystals deformed in the semi-brittle field. *Tectonophysics*, *335*, 1–15. https://doi.org/10.1016/S0040-1951(01)00042-7

Moarefvand, A., Gasc, J., Fauconnier, J., Baïsset, M., Burdette, E., Labrousse, L., & Schubnel, A. (2021). A new generation Griggs apparatus with active acoustic monitoring. *Tectonophysics*, *816*(April), 229032. https://doi.org/10.1016/j.tecto.2021.229032

Negrini, M., Stünitz, H., Nasipuri, P., Menegon, L., & Morales, L. F. G. (2014). Semibrittle deformation and partial melting of perthitic K-feldspar: An experimental study. *AGU: Journal of Geophysical Research, Solid Earth*, *119*, 3478–3502. https://doi.org/10.1002/2013JB010573

Passchier, C. W., & Trouw, R. A. J. (2005). Microtectonics. Microtectonics. https://doi.org/10.1007/3-540-29359-0

Pec, M., Stünitz, H., Heilbronner, R., Drury, M., & de Capitani, C. (2012). Origin of pseudotachylites in slow creep experiments. *Earth and Planetary Science Letters*, *355–356*, 299–310. https://doi.org/10.1016/j.epsl.2012.09.004

Pellegrino, L., Malaspina, N., Zanchetta, S., Langone, A., & Tumiati, S. (2020). High pressure melting of eclogites and metasomatism of garnet peridotites from Monte Duria Area (Central Alps, N Italy): A proxy for melt-rock reaction during subduction. *Lithos*, *358-359*, 105391. https://doi.org/10.1016/j.lithos.2020.105391

Putnis, C. V., Geisler, T., Schmid-Beurmann, P., Stephan, T., & Giampaolo, C. (2007). An experimental study of the replacement of leucite by analcime. *American Mineralogist*, *92*(1), 19–26. https://doi.org/10.2138/am.2007.2249

Renner, J., Evans, B., & Siddiqi, G. (2002). Dislocation creep of calcite. *Journal of Geophysical Research: Solid Earth*, *107*(B12), ECV 6-1–ECV 6-16. https://doi.org/10.1029/2001jb001680

Richter, B., Stünitz, H., & Heilbronner, R. (2016). Stresses and pressures at the quartz-to-coesite phase transformation in shear deformation experiments. *Journal of Geophysical Research: Solid Earth*, *121*(11), 8015–8033. https://doi.org/10.1002/2016JB013084

Rosenberg, C. L., & Handy, M. R. (2005). Experimental deformation of partially melted granite revisited: Implications for the continental crust. *Journal of Metamorphic Geology*, *23*(1), 19–28. https://doi.org/10.1111/j.1525-1314.2005.00555.x

Rowe, K. J., & Rutter, E. H. (1990). Palaeostress estimation using calcite twinning: Experimental calibration and application to nature. *Journal of Structural Geology*, *12*(1), 1–17. https://doi.org/10.1016/0191-8141(90)90044-Y

Røyne, A., Jamtveit, B., Mathiesen, J., & Malthe-Sørenssen, A. (2008). Controls on rock weathering rates by reaction-induced hierarchical fracturing. *Earth and Planetary Science Letters*, *275*(3–4), 364–369. https://doi.org/10.1016/j.epsl.2008.08.035

Rybacki, E., Gottschalk, M., Wirth, R., & Dresen, G. (2006). Influence of water fugacity and activation volume on the flow properties of fine-grained anorthite aggregates. *Journal of Geophysical Research*, *111*(December 2005), 1–16. https://doi.org/10.1029/2005JB003663

Rybacki, E., Renner, J., Konrad, K., Herbott, W., Rummel, F., & Stöckhert, B. (1998). A servohydraulically controlled deformation apparatus for rock deformation under conditions of ultra high pressure metamorphism. *Pure and Applied Geophysics*, *152*, 579–606. https://doi.org/10.1007/s000240050168

Rybacki, E., & Dresen, G. (2004). Deformation mechanism maps for feldspar rocks. *Tectonophysics*, *382*, 173–187. https://doi.org/10.1016/j.tecto.2004.01.006

Schorn, S., & Diener, J. F. A. (2017). Details of the gabbro-to-eclogite transition determined from microtextures and calculated chemical potential relationships. *Journal of Metamorphic Geology*, *35*, 55–75. https://doi.org/10.1111/jmg.12220

Smith, J. V., & Brown, W. L. (1988). *Feldspar minerals*. Springer Berlin Heidelberg. https://doi.org/10.1007/978-3-642-72594-4

Steltenpohl, M. G., Kassos, G., & Andresen, A. (2006). Retrograded eclogite-facies pseudotachylytes as deep-crustal paleoseismic faults within continental basement of Lofoten, North Norway. *Geosphere*, *2*(1), 61–72. https://doi.org/10.1130/GES00035.1

Stipp, M., Stünitz, H., Heilbronner, R., & Schmid, S. M. (2002). The eastern Tonale fault zone: A "natural laboratory" for crystal plastic deformation of quartz over a temperature range from 250 to 700°C. *Journal of Structural Geology*, *24*(12), 1861–1884. https://doi.org/10.1016/S0191-8141(02)00035-4

Stünitz, H., Fitz Gerald, J. D., & Tullis, J. (2003). Dislocation generation, slip systems, and dynamic recrystallization in experimentally deformed plagioclase single crystals. *Tectonophysics*, *372*, 215–233. https://doi.org/10.1016/S0040-1951(03)00241-5

Stünitz, H., Neufeld, K., Heilbronner, R., Finstad, A. K., Konopásek, J., & Mackenzie, J. R. (2020). Transformation weakening: Diffusion creep in eclogites as a result of interaction of mineral reactions and deformation. *Journal of Structural Geology*, *139*, 104129. https://doi.org/10.1016/j.jsg.2020.104129

Stünitz, H., & Tullis, J. (2001). Weakening and strain localization produced by syn-deformational reaction of plagioclase. *International Journal of Earth Sciences*, *90*(1), 136–148. https://doi.org/10.1007/s005310000148

Tajčmanová, L., Podladchikov, Y., Powell, R., Moulas, E., Vrijmoed, J. C., & Connolly, J. A. D. (2014). Grain-scale pressure variations and chemical equilibrium in high-grade metamorphic rocks. *Journal of Metamorphic Geology*, *32*(2), 195–207. https://doi.org/10.1111/jmg.12066

Tsuchiyama, A., & Takahashi, E. (1983). Melting kinetics of a plagioclase feldspar. *Contributions to Mineralogy and Petrology*, *84*(4), 345–354. https://doi.org/10.1007/BF01160286

Tullis, J. (2018). Deformation of feldspars. In P. H. Ribbe (Ed.). *Feldspar mineralogy* (pp. 297–323). De Gruyter. https://doi.org/10.1515/9781501508547-018

Tullis, J., & Yund, R. (1992). The brittle-ductile transition in feldspar aggregates: An experimental study. *International Geophysics*, *51*(C), 89–117. https://doi.org/10.1016/S0074-6142(08)62816-8

Tullis, J., & Yund, R. A. (1987). Transition from cataclastic flow to dislocation creep of feldspar: Mechanisms and microstructures. *Geology*, *15*(7), 606–609. https://doi.org/10.1130/0091-7613(1987)15<606:TFCFTD>2.0.CO

Vrijmoed, J. C., Podladchikov, Y. Y., Andersen, T. B., & Hartz, E. H. (2009). An alternative model for ultra-high pressure in the Svartberget Fe-Ti garnet-peridotite, Western Gneiss Region, Norway. *European Journal of Mineralogy*, *21*(6), 1119–1133. https://doi.org/10.1127/0935-1221/2009/0021-1985

Wang, S. J., Wang, L., Brown, M., Johnson, T. E., Piccoli, P. M., Feng, P., & Wang, Z. L. (2020). Petrogenesis of leucosome sheets in migmatitic UHP eclogites—Evolution from silicate-rich supercritical fluid to hydrous melt. *Lithos*, *360-361*, 105442. https://doi.org/10.1016/j.lithos.2020.105442

Wang, Y., Durham, W. B., Getting, I. C., & Weidner, D. J. (2003). The deformation-DIA: A new apparatus for high temperature triaxial deformation to pressures up to 15 GPa. *Review of Scientific Instruments*, *74*(6), 3002–3011. https://doi.org/10.1063/1.1570948

Wayte, G. J., Worden, R. H., Rubie, D. C., & Droop, G. T. R. (1989). A TEM study of disequilibrium plagioclase breakdown at high pressure: The role of infiltrating fluid. *Contributions to Mineralogy and Petrology*, *101*(4), 426–437. https://doi.org/10.1007/BF00372216

White, R. W., Powell, R., & Holland, T. J. B. (2001). Calculation of partial melting equilibria in the system. *Journal of Metamorphic Geology*, *19*(2), 139–153. https://doi.org/10.1046/j.0263-4929.2000.00303.x

Whitney, D. L., & Evans, B. W. (2010). Abbreviations for names of rock-forming minerals. *American Mineralogist*, *95*(1), 185–187. https://doi.org/10.2138/am.2010.3371

Xie, D., Hirth, G., Hirth, J. P., & Wang, J. (2019). Defects in deformation twins in plagioclase. *Physics and Chemistry of Minerals*, *46*(10), 959–975. https://doi.org/10.1007/s00269-019-01055-9

Yund, R. A., Blanpied, M. L., Tullis, T. E., & Weeks, J. D. (1990). Amorphous material in high strain experimental fault gouges. *Journal of Geophysical Research*, *95*(B10), 15589–15602. https://doi.org/10.1029/JB095iB10p15589

How to cite this article: Incel, S., Baïsset, M., Labrousse, L., & Schubnel, A. (2023). Partial melting and reaction along deformation features in plagioclase. *Journal of Metamorphic Geology*, *41*(3), 449–464. https://doi.org/10.1111/jmg.12702